# Enrichment and characterization of ammonia-oxidizing archaea from the open ocean: Phylogeny, physiology, and stable isotope fractionation

Alyson E. Santoro[1,2]* and Karen L. Casciotti[1,3]

A manuscript for: *ISME Journal*

Running head: Isotope fractionation by ammonia-oxidizing archaea

[1]Department of Marine Chemistry and Geochemistry, Woods Hole Oceanographic Institution, Woods Hole, Massachusetts, 02543, USA

[2]Present address: Horn Point Laboratory, University of Maryland Center for Environmental Science, Cambridge, Maryland, 21613, USA

[3]Present address: Department of Environmental Earth System Science, Stanford University, Stanford, California, 94305, USA

*Corresponding author: asantoro@umces.edu

**Abstract**

Archaeal genes for ammonia oxidation are widespread in the marine environment, but direct physiological evidence for ammonia oxidation by marine archaea is limited. We report the enrichment and characterization of three strains of pelagic ammonia-oxidizing archaea (AOA) from the north Pacific Ocean that have been maintained in laboratory culture for over three years. Phylogenetic analyses indicate the three strains belong to a previously identified clade of water column-associated AOA and possess 16S rRNA genes and ammonia monooxygenase subunit a (*amoA*) genes highly similar (98-99% identity) to those recovered in DNA and cDNA clone libraries from the open ocean. The strains grow in natural seawater-based liquid medium while stoichiometrically converting ammonium ($NH_4^+$) to nitrite ($NO_2^-$). Ammonia oxidation by the enrichments is only partially inhibited by allylthiourea at concentrations known to inhibit cultivated ammonia-oxidizing bacteria. The three strains were used to determine the nitrogen stable isotope effect ($^{15}\varepsilon_{NH3}$) during archaeal ammonia oxidation, an important parameter for interpreting stable isotope ratios in the environment. Archaeal $^{15}\varepsilon_{NH3}$ ranged from 13-41‰, within the range of that previously reported for ammonia-oxidizing bacteria. Despite low amino acid identity between the archaeal and bacterial Amo proteins, their functional diversity as captured by $^{15}\varepsilon_{NH3}$ is similar.

## Introduction

Mesophilic archaea are ubiquitous and abundant members of diverse marine environments including coastal waters (Beman *et al.*, 2010; Mincer *et al.*, 2007, and references therein), marine sediments, estuaries (Bernhard *et al.*, 2010; Mosier and Francis, 2008; Urakawa *et al.*, 2010), stratified basins (Coolen *et al.*, 2007; Lam *et al.*, 2007) and open ocean water columns (Beman *et al.*, 2008; Church *et al.*, 2010; Santoro *et al.*, 2010). The recent cultivation of the first mesophilic marine archaeon, *Nitrosopumilus maritimus*, (Konneke *et al.*, 2005; Martens-Habbena *et al.*, 2009), two thermophilic archaea, *Nitrosocaldus yellowstonii* and *Nitrosophaera gargensis* (de la Torre *et al.*, 2008; Hatzenpichler *et al.*, 2008), and a freshwater archaeon, *Nitrosoarchaeum limnia* (Blainey *et al.*, 2011) established that at least some of these organisms are chemolithoautotrophic ammonia oxidizers. Several studies coupling gene- and cell-based quantification of putative ammonia-oxidizing archaea (AOA) to rate measurements (Beman *et al.*, 2008; Santoro *et al.*, 2010; Wuchter *et al.*, 2006) suggest that nitrification by AOA in the ocean is significant. However, direct demonstration of ammonia-oxidizing activity by the AOA genotypes encountered in the open ocean has not yet been demonstrated.

Ammonia oxidation is the first step of nitrification, a key remineralization reaction in the sea. Work by Olsen (1981) and Ward et al. (1982) using $^{15}N$ isotope tracers first suggested that nitrification in the upper ocean could be a significant source of regenerated nutrients for primary production. The quantitative role, however, of nitrification in the euphotic zone is still uncertain. Recent syntheses of nitrification rates made using isotope tracers (Clark *et al.*, 2008; Yool *et al.*, 2007) suggest that globally,

nitrification may be a significant source of regenerated N for primary production, supplying as much as half of the necessary nitrate. This has important implications for estimates of carbon export based on new production (Eppley and Peterson, 1979); an underestimation of nutrient regeneration would lead to an overestimation of export from the surface ocean (Ward, 2002).

Though instantaneous rate measurements with $^{15}$N-labeled compounds provide important insights into the environmental controls on nitrification, they capture only a 'snapshot' view of this undoubtedly time-varying process. An alternative way of quantifying the importance of nitrification is using natural abundance stable isotope ratios to infer the relative importance of different nitrogen cycling processes. In particular, nitrogen and oxygen stable isotope ratios ($\delta^{15}$N and $\delta^{18}$O) in marine nitrate ($NO_3^-$) can integrate information about the relative sources (nitrification, upward diffusion, atmospheric deposition) and sinks (phytoplankton uptake) of $NO_3^-$ in the euphotic zone (Casciotti *et al.*, 2008; DiFiore *et al.*, 2009; Sigman *et al.*, 2005; Wankel *et al.*, 2007) and provide an independent constraint on the importance of nitrification to new production. In order to interpret these measurements, however, the isotope effects for the various sources and sinks of $NO_3^-$ must be known. The isotope effects for $NO_3^-$ uptake by phytoplankton (Granger *et al.*, 2004; Needoba *et al.*, 2003) and $NO_2^-$ production by nitrifying bacteria (Casciotti *et al.*, 2010; Casciotti *et al.*, 2003; Mariotti *et al.*, 1981) are relatively well studied, but there are no data on the isotope effects for ammonia oxidation by AOA.

In this study we describe the enrichment and characterization of three strains of AOA from the water column of the North Eastern Pacific Ocean that oxidize $NH_3$ to

$NO_2^-$. We used the three strains to estimate the nitrogen kinetic isotope effect ($^{15}\varepsilon_{NH3}$) during ammonia oxidation by AOA. Our results extend the ability for chemoautotrophic ammonia oxidation within the *Archaea* and expand the number of marine archaea for which we have both phylogeny and confirmed metabolic function. We provide important constraints for the interpretation of natural abundance stable isotope ratios for these ubiquitous organisms in the marine nitrogen cycle.

## Materials and Methods

*Enrichment and cultivation*. Enrichment cultures were initiated with water from the North Eastern Pacific approximately 300 km from shore (California Cooperative Oceanic Fisheries Investigations station 67-90; 35.46ºN, 124.91ºW) aboard the R/V *Western Flyer* during cruise CN107 in July 2007 (Table 1). Seawater was collected from 25 m, 75 m, 150 m, and 500 m depths using a standard 10 L Niskin rosette sampler equipped with a conductivity-temperature-depth sensor package. Seawater was stored at 22ºC (25 m and 75 m waters) and 4ºC (150 m and 500 m waters) in 500 mL acid-cleaned polycarbonate bottles. After 20 months of incubation, filter sterile ammonium chloride ($NH_4Cl$) was added to a final concentration of 10 µmol $L^{-1}$ and the enrichments were monitored for production of $NO_2^-$ using standard colorimetric methods (Strickland and Parsons, 1968). At that time, the 150 m enrichment was moved to 13ºC and maintained at that temperature. Hereafter, the successful enrichments are referred to as CN25, CN75, and CN150 referring to the cruise name and depth of the enrichment inoculums.

Cultures were maintained with transfers of 10 - 20% (v/v) late exponential phase culture into oligotrophic North Pacific (ONP) medium consisting of: 0.2 µm-filtered

North Pacific surface seawater amended with 10-100 µmol $L^{-1}$ $NH_4Cl$, 1 mL $L^{-1}$ chelated trace elements solution (Balch *et al.*, 1979), 15 µmol $L^{-1}$ $KH_2PO_4$ and 100 µg $mL^{-1}$ each streptomycin and ampicillin. Maintenance cultures were grown in 200 mL volumes in 250 mL acid-cleaned polycarbonate bottles. Surface seawater for ONP medium was obtained either from the initial collection site or from the Pacific hydrographic station SAFe (Johnson *et al.*, 2007).

Abundance of archaeal and bacterial cells in the enrichments was periodically monitored in 1 mL formaldehyde-fixed culture volumes filtered onto 25 mm diameter, 0.2 µm pore size polycarbonate filters (Millipore GTTP, Billerica, MA, USA) with catalyzed auto reporter deposition-fluorescent in situ hybridization (CARD-FISH) and epifluorescence microscopy using probes Cren537-554 and EUB338 I-III (Teira *et al.*, 2004).

*Phylogenetic analysis of 16S rRNA and* amoA *genes*. DNA was extracted and purified from 25 mL of culture after vacuum filtration onto 25 mm diameter, 0.2 µm pore size Supor membrane filters (Pall, Port Washington, NY, USA) using DNeasy columns (Qiagen, Valencia, CA, USA) as previously described (Santoro *et al.*, 2008). Genes encoding for the 16S rRNA and the $\alpha$ subunit of ammonia monooxygenase (*amoA*), believed to contain the catalytic site for ammonia oxidation (Hyman and Wood, 1985), were amplified using PCR. Target genes were amplified in 25 µL PCR reactions using the primers: 21F/1492R (archaeal 16S rRNA genes, DeLong (1992)), ArchamoAF/ArchamoAR (archaeal *amoA*, Francis *et al*. 2005), 27F/1492R (bacterial 16S rRNA), and amoAF*/amoAR (betaproteobacterial *amoA*, Stephen *et al.* (1999)) using reaction and thermocycling conditions described in the original manuscripts or as

modified in Santoro *et al.* (2010). Gammaproteobacterial *amoA* genes were amplified using the amoA3F/amoB4R primer set (Purkhold *et al.*, 2000) using the following thermocycling profile: 95ºC for 3 min followed by 35 cycles of : 95ºC for 30 sec, 50ºC for 45 sec, and 72ºC for 1 min. Genomic DNA from *Nitrosococcus oceani* was used as a positive control. PCR products were pooled, purified (MinElute PCR Purification Kit, Qiagen), and cloned using the TOPO-TA cloning kit with pCR4 vector and MACH1 competent cells (Invitrogen, Carlsbad, CA, USA). Plasmids were purified (Mini Prep Spin Kit, Qiagen) and sequenced on an ABI 3730xl sequencer. Twelve archaeal 16S rRNA and *amoA* clones and 24 bacterial 16S rRNA clones were sequenced per enrichment.

16S rRNA gene sequences were imported into the ARB software program (Ludwig *et al.*, 2004) and aligned to a subset of the SILVA SSU reference database, Feb 2009 release (Pruesse *et al.*, 2007). Archaeal *amoA* sequences were manually aligned and imported into an ARB database maintained by our laboratory containing approximately 2000 environmental *amoA* sequences. Phylogenetic trees were constructed using 1,268 nucleotide positions (16S rRNA) or 489 nucleotide positions (*amoA*) using maximum likelihood (RAxML) analyses implemented using the Cyberinfrastructure for Phylogenetic Research (CIPRES) Portal v3.0 (www.phylo.org) and visualized using FigTree v1.3.1 (http://tree.bio.ed.ac.uk/software/figtree/). Archaeal 16S rRNA gene and *amoA* sequences from this study were deposited in GenBank under the accession numbers HQ338108-HQ338109 and JF521547-JF521549.

*Growth curves*. Growth curves were determined for CN25 and CN75 at 22ºC in replicate 200 mL volumes of ONP medium containing 50 µmol $L^{-1}$ $NH_4^+$. At each time point, 15

mL of culture was removed. Ten milliliters of culture were frozen for later [$NO_2^-$] and [$NH_4^+$] determination. The remaining 5 mL of culture were immediately fixed with formaldehyde (2% final concentration) for four hours and replicate volumes (0.5 – 2 mL) of fixed culture were vacuum filtered onto 25 mm, 0.2 µm pore size polycarbonate membrane filters (Millipore) and frozen for later CARD-FISH analysis as described above. A minimum of ten fields of view were counted from each filter using the 100X objective on a Zeiss Axio Scope epifluorescence microscope. [$NH_4^+$] and [$NO_2^-$] determinations were made in duplicate using phthaldialdehyde fluorescence (Holmes *et al.*, 1999) and azo dye colorimetry (Strickland and Parsons, 1968), respectively.

*Allylthiourea inhibition experiments*. To assess the effect of the metal chelator allylthiourea (ATU) on archaeal ammonia oxidation, strain CN25 was grown in triplicate 50 mL volumes in 60 mL polycarbonate screw cap bottles for each of three treatments: no ATU addition (control), 10 mg $L^{-1}$ ATU (86 µmol $L^{-1}$), and 100 mg $L^{-1}$ (860 µmol $L^{-1}$). ATU additions were made from a 10 mg $mL^{-1}$ stock solution of ATU (Sigma) dissolved in water. Ammonia oxidation was monitored by the production of $NO_2^-$, determined using azo dye colorimetry in 1 mL volumes (Strickland and Parsons, 1968). ATU was added to the treatment bottles after initial $NO_2^-$ production was detected in each flask (day 4). Inhibition for the ATU treatments was calculated as the percent decrease in slope of a linear regression fit to the ln[$NO_2^-$] over time compared with the control bottles.

*Nitrogen isotope effect estimates*. For each experiment, 25 mL of enrichment culture was inoculated into 175 mL of ONP medium containing 10-25 µmol $L^{-1}$ $NH_4^+$ in a 250 mL acid-washed, screw-cap polycarbonate bottle. Growth was not observed when

experiments were initiated with washed cell suspensions collected by filtration (data not shown), thus all experiments started with an initial [$NO_2^-$] between 2 and 10 µmol $L^{-1}$ as well as residual $NH_4^+$ from maintenance cultures, in some cases. Temperature was maintained at 22 ˚C for CN25 and CN75 and 13 ˚C for CN150. $NO_2^-$ production was monitored and 15 mL of enrichment culture was removed at each time point and frozen at -20ºC.

Initial and time-course measurements of [$NH_4^+$] and [$NO_2^-$] were made in duplicate using phthaldialdehyde fluorescence (Holmes *et al.*, 1999) and azo dye colorimetry (Strickland and Parsons, 1968), respectively, on 2 mL sample volumes. Error in replicate [$NH_4^+$] analyses ranged from 2-7%; error in replicate [$NO_2^-$] analyses was 0-8%. Isotopic measurements of $NO_2^-$ were made by converting $NO_2^-$ to $N_2O$ using the 'azide method' (McIlvin and Altabet, 2005) with 10-20 nmol N per sample. The resulting $N_2O$ was captured using a custom purge and cryogenic trapping system (Casciotti *et al.*, 2002; McIlvin and Casciotti, 2010; McIlvin and Casciotti, 2011) and analyzed using a Finnigan Delta$^{PLUS}$ XP isotope ratio mass spectrometer. Each sample was analyzed in duplicate against RSIL nitrite reference materials N23, N7373, and N10219 run in parallel (Casciotti *et al.*, 2007). Results are reported using delta notation: $\delta^{15}N_{NO2}$ (‰ vs. AIR) = [($^{15}R_{NO2}$ / $^{15}R_{AIR}$) -1] x 1000, where $^{15}R = {}^{15}N:{}^{14}N$ and AIR is standard atmospheric $N_2$. Error in replicate measurements of $\delta^{15}N_{NO2}$ was 0.3‰ or better for all experiments.

Calculation of $^{15}\varepsilon_{NH3}$ requires knowledge of the isotopic composition of the $NO_2^-$ produced over time since an arbitrary starting point. If the initial [$NO_2^-$] is zero, then the measured $\delta^{15}N_{NO2}$ ($\delta^{15}N_{NO2total}$) is equal to that produced ($\delta^{15}N_{NO2produced}$). If there is

$NO_2^-$ initially present, as in our experiments, the $\delta^{15}N_{NO2produced}$ at any time since the initial time point (*i*) must be calculated from $\delta^{15}N_{NO2total}$ using the following equations:

$$(^{15}N:^{14}N)_{total} * [NO_2^-]_{total} = (^{15}N:^{14}N)_{produced} * [NO_2^-]_{produced} + (^{15}N:^{14}N)_i * [NO_2^-]_i \quad \text{Eq (1a)}$$

where $(^{15}N:^{14}N)_{total} = (^{15}N:^{14}N)_{AIR} * (\delta^{15}N_{NO2total}/1000 + 1)$

Rearranging:

$$(^{15}N:^{14}N)_{produced} = \{(^{15}N:^{14}N)_{total} * [NO_2^-]_{total} - (^{15}N:^{14}N)_i * [NO_2^-]_i\} / [NO_2\text{-}]_{produced} \quad \text{Eq (1b)}$$

$$\delta^{15}N_{NO2produced} = [(^{15}N:^{14}N)_{produced}/(^{15}N:^{14}N)_{AIR} - 1] * 1000 \qquad \text{Eq (2)}$$

The isotope effect ($^{15}\varepsilon_{NH3}$) was then calculated from the $\delta^{15}N_{NO2produced}$ data using the Rayleigh accumulated product equation (after Mariotti *et al*., 1981):

$$\delta^{15}N_{NO2_{produced}} = \delta^{15}N_{NH4_{initial}} + {}^{15}\varepsilon_{NH3}\left(\frac{f\ln(f)}{1-f}\right) \qquad \text{Eq (3)}$$

where $f = [NH_4^+]/[NH_4^+]_{initial}$. By Eq (3), the slope of a best fit line on a plot of $\delta^{15}N_{NO2}$ vs. $f$ *ln($f$)/(1-$f$) yields $^{15}\varepsilon_{NH3}$ and the *y*-intercept corresponds to the starting $\delta^{15}N_{NH4}$. Because each experiment was initiated with a mixture of $NH_4^+$ carried over from the enrichment transfer and 'new' $NH_4^+$ from freshly prepared medium ($\delta^{15}N \sim -3‰$), minor variations in the $\delta^{15}N_{NH4}$ (and the *y*-intercept) are expected between experiments and therefore each experiment was fitted separately. Fitting and 95% confidence interval calculations were done using IGOR Pro software (v5, WaveMetrics, Inc., Lake Oswego, OR, USA).

Use of the Rayleigh model presumes that ammonia oxidation proceeds as a pseudo one-step reaction with no accumulation of an intermediate product between $NH_3$ and $NO_2^-$ and no back-reaction of the products (Casciotti *et al.*, 2003). When estimated

in this way, several isotope effects are incorporated into $^{15}\varepsilon_{NH3}$ including a ~20-35‰ equilibrium isotope effect between $NH_4^+$ and $NH_3$ (Casciotti *et al.*, 2011), as well as any isotope effects for $NH_3$ or $NH_4^+$ diffusion. Errors in $^{15}\varepsilon_{NH3}$ resulting from these assumptions, as well as errors resulting from uncertainties in the archaeal ammonia oxidation pathway, are discussed below.

**Results**

*Phylogeny and physiology*. Following 20 months of incubation in the dark with no amendments, archaeal *amoA* genes were detected by PCR in all four seawater 'enrichment' bottles (25 m, 75 m, 150 m, and 500 m). On addition of 10 µmol $L^{-1}$ $NH_4^+$, $NO_2^-$ production was observed in the enrichments from 25 m, 75 m, and 150 m within one month (data not shown). No $NO_2^-$ production was observed in the 500 m bottle. The $NO_2^-$ producing enrichments are referred to as CN25, CN75, and CN150. All three CN enrichments contained a high proportion of cells hybridizing with the CARD-FISH probe suite CREN537-554 and PCR amplifiable archaeal *amoA* genes. No *amoA* genes from either gamma or betaproteobacteria were detected.

After approximately one year of routine transfers into ONP medium (nearly three years after initial collection), the enrichments were highly enriched in archaeal cells (Fig. 1) and the basic phylogeny and physiology of the enrichments were characterized. A consensus archaeal 16S rRNA gene sequence was obtained from 12 clones from each enrichment. One sequence from CN25 and two sequences from CN75 contained single nucleotide changes (all at different positions) from this consensus sequence. Phylogenetic analyses place all three sequences within the Marine Group I archaea, now

proposed as a new archaeal kingdom—the Thaumarchaeota (Brochier-Armanet *et al.*, 2008; Spang *et al.*, 2010; Walker *et al.*, 2010)(Fig. 2a). The 16S rRNA gene sequences from CN25 and CN75 are 100% identical to each other, and 92% identical to *N. maritimus*. Closest GenBank BLAST matches to the CN25 16S rRNA gene sequence are 98% identical and include sequences from environmental clone libraries from 200 m depth off the Oregon coast (fosmid 4B7, U40238, (Stein *et al.*, 1996)) and an unpublished deep sea hydrothermal vent clone from Suiyo Seamount (AB194001). The CN150 16S rRNA gene is 98% identical to *N. maritimus* and 99% identical to several sequences from the Sargasso Sea metagenome (AACY020033564, (Venter *et al.*, 2004)).

The *amoA* sequences from CN25 and CN75 fall within a cluster of environmental sequences previously termed water column cluster 'A.' They are also 100% identical at the amino acid level to several sequences from the Sargasso Sea metagenome (Venter *et al.*, 2004)(Fig. 2b) and 84% and 95% identical at the nucleotide and amino acid levels, respectively, to the *amoA* sequence from *N. maritimus*. The CN150 *amoA* gene is also 84% identical to *N. maritimus* at the nucleic acid level. Because CN25 and CN75 are identical at the 16S rRNA and *amoA* level, full genome sequencing may be necessary to resolve any strain-level differences between the two enrichments.

Bacterial 16S rRNA gene clone libraries from the CN enrichments did not contain 16S rRNA genes from any genera of known bacterial nitrifiers and contained sequences associated with the genera *Erythrobacter* and *Gracilimonas*. Bacterial *amoA* genes could not be detected using PCR amplification.

Stoichiometric conversion of $NH_4^+$ to $NO_2^-$ was observed in all three enrichments coincident with an exponential increase in the number of archaeal cells, evidence that the

CN strains couple ammonia oxidation to growth (Fig. 3). All three CN strains were able to utilize $NH_4^+$ from the medium below our detection limit of ~200 nM. Bacterial cells, as quantified by CARD-FISH, were not detectible until the archaeal population entered late exponential-early stationary phase. CN25 and CN75, growing at 22ºC, had lag phases of 4-10 days upon transferring 10 – 25% of the original culture volume into new medium, even when cultures were transferred during exponential phase growth. Transfer volumes of less than 10% failed to grow (data not shown). CN150, growing at 13ºC, had lag phases of up to 25 days.

CN25 and CN75 were chosen for more detailed growth studies due to faster $NH_4^+$ oxidation rates, shorter lag phases, and more consistent growth. The CN25 growth rate at 22ºC was 0.15 $d^{-1}$; the CN75 growth rate was 0.17 $d^{-1}$, corresponding to doubling times of about 4-4.6 d. Stationary phase cell densities in CN25 and CN75 were 2.7 - 3.2 x $10^6$ cells $mL^{-1}$ with 86-97% of cells hybridizing with archaeal CARD-FISH probes depending on the growth stage of the enrichment.

Allythiourea (ATU) is frequently used to inhibit nitrifying activity in environmental studies. We tested the effect of ATU on the ammonia oxidation rate for CN25. An ATU concentration of 10 mg $L^{-1}$ (86 µmol $L^{-1}$) inhibited the ammonia oxidation rate by 58%; an ATU concentration of 100 mg $L^{-1}$ (860 µmol $L^{-1}$) completely inhibited ammonia oxidation (Fig. 4).

*Nitrogen isotopic fractionation*. To further investigate the physiology of the enriched strains, we determined their N kinetic isotope effect during ammonia oxidation ($^{15}\varepsilon_{NH3}$). As in growth curve experiments, we observed near stoichiometric conversion of $NH_4^+$ to

$NO_2^-$ over the course of the isotope fractionation experiments, with conservation in the DIN pool ($NH_4^+ + NO_2^-$) ranging from 74% to 107% with a mean of 97% (Table 2).

Results from replicate experiments are reported individually, as well as an unweighted average of experiments for a given enrichment (Table 2). $^{15}\varepsilon_{NH3}$ for CN25 ranged from 14-30‰ with an average of 22 ± 5‰ ($n$ = 11), $^{15}\varepsilon_{NH3}$ for CN75 ranged from 10-37‰ with an average of 21 ± 10‰ ($n$ = 6), and $^{15}\varepsilon_{NH3}$ for CN150 ranged from 16-28‰ with an average of 22 ± 5‰ ($n$ = 7). Non-linearity was observed in most experiments with CN25 and CN75, with larger $^{15}\varepsilon_{NH3}$ (i.e. greater slopes) at the beginning of the growth curve when a large fraction ($f$) of the initial $NH_4^+$ remained (Fig. 5a,b). This leads to large uncertainties (expressed as 95% confidence intervals) in the slopes for many of the experiments with CN25 and CN75 (Table 2). We did not observe the same non-linearity of $^{15}\varepsilon_{NH3}$ in experiments with CN150 (Fig. 5c).

## Discussion

*Phylogeny*. We established three enrichments of marine archaea that stoichiometrically oxidize $NH_4^+$ to $NO_2^-$. Multiple lines of evidence suggest that the archaea are the active ammonia oxidizers in the enrichments. Archaeal cells increase exponentially concomitant with an exponential increase in $NO_2^-$ and *amoA* genes from the enrichments have a high identity to known archaeal ammonia oxidizers. The enrichments lack 16S rRNA and *amoA* genes associated with known γ- or β-proteobacterial ammonia-oxidizers. Though no $NO_2^-$ or $NO_3^-$ production was observed in the enrichment from 500 m, this cannot be used to infer a lack of $NH_3$-oxidizing ability in field populations at this depth as active $NH_3$ oxidation was measured in situ (Santoro *et al.*, 2010).

Both 16S rRNA and *amoA* gene sequences from the CN strains suggest they are representative of organisms present and active in the open ocean. CN25 and CN75 are 97% identical to *amoA* sequences obtained in DNA-based clone libraries from the environment from which they were enriched (GU360825, (Santoro *et al.*, 2010)) and CN150 is 100% identical to an *amoA* actively expressed in the environment (GU364088). The CN strains are also highly similar on the 16S and *amoA* level to abundant groups of open ocean archaea from a range of oceanic provinces including the Sargasso Sea, Fernandina Island, and the coast of Africa as indicated by BLAST searches of the Global Ocean Survey dataset (Rusch *et al.*, 2007). Previous *amoA*-based phylogenies of AOA have shown that water column-derived sequences fall into two clusters termed 'A' and 'B' (Francis *et al.*, 2005) thought to represent a depth-dependent partitioning of AOA (Beman *et al.*, 2008; Hallam *et al.*, 2006; Mincer *et al.*, 2007). The exact physiological basis for the partitioning of archaeal *amoA* genotypes is unknown but could include adaptations to temperature, light, or substrate availability. Based on *amoA* sequences, all three CN strains belong to the shallow water column clade 'A.' Our data now associate a 16S rRNA genotype with at least some members of the clade 'A' archaea distinct from *N. maritimus* that are likely to represent a new genus within the Thaumarchaea.

*Physiology.* The growth rate of CN25 and CN75 (0.17 $d^{-1}$) in ONP medium is slower than growth rates reported for the cultivated AOA *N. maritimus* (0.65 $d^{-1}$ at 30ºC, (Martens-Habbena *et al.*, 2009) and *N. yellowstonii* (0.8 $d^{-1}$ at 72ºC, (de la Torre *et al.*, 2008) and cultivated marine AOB (0.34 – 0.77 $d^{-1}$, (Prosser, 1990). These differences can be partially explained by the lower cultivation temperature of the CN enrichments (22ºC)

relative to *N. maritimus* and *N. yellowstonii*. Further optimization of the culture medium may lead to increases in the growth rates reported here. The per-cell activity rate for the CN strains, ~2 fmol $NO_2^-$ $cell^{-1}$ $d^{-1}$, is lower than *N. maritimus* (13 fmol $cell^{-1}$ $d^{-1}$, (Martens-Habbena *et al.*, 2009)), but similar to a mesocosm enrichment of archaea from North Atlantic (2-4 fmol $cell^{-1}$ $d^{-1}$)(Wuchter *et al.*, 2006), and estimates of *in situ* per-cell activity rates in the California Current (0.2-15 fmol $cell^{-1}$ $d^{-1}$) (Santoro *et al.*, 2010).

Multiple isolation strategies, including the addition of antibiotics and size fractionation through 0.45 µm filters, did not yield pure cultures of any of the CN strains. Dilution-to-extinction approaches were also not successful, as high dilutions of the CN strains did not grow (data not shown). *N. yellowstonii* and *N. gargensis*, the two cultivated thermophilic strains of AOA, also could not be established in pure culture (de la Torre *et al.*, 2008; Hatzenpichler *et al.*, 2008). This may be because there is a cooperative relationship between the bacteria and the archaea in these enrichment cultures, as has been reported in cultures of the marine chlorophyte *Prochlorococcus*, (Morris *et al.*, 2008) and low cell density dilutions that do not contain the associated heterotrophic bacteria are unable to grow. Interactions between the heterotrophic bacteria and autotrophic archaea in the enrichment, and in the ocean, will be an exciting area of future research.

We observed partial inhibition of archaeal ammonia-oxidizing activity by ATU at 86 µmol $L^{-1}$, a concentration known to completely inhibit cultivated AOB (Hooper and Terry, 1973) and bacterial-rich environmental samples (Ginestet *et al.*, 1998), and near complete inhibition of ammonia oxidation in CN25 was observed at 860 µmol $L^{-1}$ ATU. The mechanism of ATU inhibition in AOB is thought to be chelation of the Cu active site

in the Amo protein (Bedard and Knowles, 1989). Our results are consistent with observations of *N. gargensis* (Hatzenpichler *et al.*, 2008) and support the idea that ATU-inhibited rates may represent conservative estimates of AOA-only activity in the field. Further, these results suggest that ATU should not be relied on for complete inhibition of nitrifying activity in environmental samples. For example, nitrification rate measurements in the California Current showed variable (0-90%) but on average low levels of inhibition by ATU (mean 35%, $n = 11$) consistent with other lines of evidence supporting AOA activity in that study (Santoro *et al.*, 2010). On the other hand, Lam *et al*. (2009) reported complete inhibition of ammonium oxidation in the presence of 86 μmol $L^{-1}$ ATU in the Eastern Tropical South Pacific oxygen minimum zone. The physiology behind the differential response of AOA and AOB and different environmental communities to this inhibitor is unknown, but could be the result of different metal active sites for enzymes in the ammonia oxidation pathway between the two groups of organisms or differences in trace metal availability or trace metal affinity in different field locations.

*Nitrogen isotopic fractionation.* Multiple experiments with the three archaeal enrichments suggest a $^{15}\varepsilon_{NH3}$ for archaeal ammonia oxidation of approximately 22‰. This value falls within the reported $^{15}\varepsilon_{NH3}$ for bacterial ammonia oxidation of 14 to 42‰ (Casciotti *et al.*, 2010; Casciotti *et al.*, 2003; Mariotti *et al.*, 1981). Thus, despite genome-inferred differences in the ammonia oxidation pathways of AOA and AOB (Walker *et al.*, 2010), a difference in the magnitude of $^{15}\varepsilon_{NH3}$ between these two groups was not apparent.

The physiological reasons for the large range in $^{15}\varepsilon_{NH3}$ for both AOA and AOB are unknown, but could result from changes in growth state of the organisms or violations of assumptions associated with using the accumulated product equation to estimate $^{15}\varepsilon_{NH3}$ from $\delta^{15}N_{NO2}$ measurements. Factors to consider include variations in substrate concentration, ammonia oxidation rate, and loss of N to unmeasured pools. Furthermore, unbalanced growth could lead to accumulation of intermediate products in the multi-step oxidation pathway, leading to larger errors involved with characterization of ammonia oxidation as a single-step unidirectional reaction. At high starting [$NH_4^+$], expressed $^{15}\varepsilon_{NH3}$ values were consistently around 20-22‰, whereas at low starting [$NH_4^+$], expressed $^{15}\varepsilon_{NH3}$ values were more variable (both higher and lower) and greater uncertainty was involved in their estimation (Table 2). Therefore, no direct relationship can be drawn between [$NH_4^+$] and $^{15}\varepsilon_{NH3.}$ Likewise, there is no direct relationship between ammonia oxidation rate (or oxidation rate/[$NH_4^+$]) and $^{15}\varepsilon_{NH3}$ (Table 2).

Though DIN conservation ([$NH_4^+ + NO_2^-$]) was not 100% in all experiments, the majority of experiments had $NO_2^-$ recoveries over 90% (Table 2), which is within the range reported for pure cultures of AOB (Casciotti *et al.*, 2002; Mariotti *et al.*, 1981). There is likely to be some loss of $NH_4^+$ due to uptake for anabolic metabolism by AOA and the bacteria in the enrichments, but this sink should be small and consistent across experiments. This process could alter observed $^{15}\varepsilon_{NH3}$ values in proportion to the amount of $NH_4^+$ assimilated and the isotope effect for $NH_4^+$ assimilation (4-27‰; (Hoch *et al.*, 1992)). However, we emphasize that this effect is likely to be small and note that relatively high estimates of $^{15}\varepsilon_{NH3}$, not low ones, were observed where recovery was low (Table 2). We did not make measurements of [$NO_3^-$] in the experiments described here,

but we have not observed $NO_2^-$ loss over time and have no evidence that $NO_2^-$ is further oxidized to $NO_3^-$ in any of the enrichments.

In addition to variation between experiments, we found evidence for variable $^{15}\varepsilon_{NH3}$ during archaeal ammonia oxidation within some experiments, with the greatest $^{15}\varepsilon_{NH3}$ expressed at the early stages of growth. This was particularly apparent for CN25 and CN75 grown at low [$NH_4^+$] (<20 μM), which exhibited a considerable lag phase prior to the commencement of ammonia oxidation. Variable $\varepsilon$ values have been observed in many other organisms, including denitrifiers (Granger *et al.*, 2008), methane oxidizers (Templeton *et al.*, 2006), sulfate reducers (Habicht *et al.*, 2005) and nitrite oxidizers (Buchwald and Casciotti, 2010; Casciotti, 2009), and during assimilation of $NH_4^+$ by heterotrophic bacteria (Hoch *et al.*, 1992) but has not previously been reported in ammonia-oxidizing organisms. We explore two hypotheses that could explain a large apparent isotope effect at the early stages of growth (Fig. 6).

The first hypothesis is that, in the early stages of growth in batch culture, diffusion of $NH_3$ and/or $NH_4^+$ between the periplasm and the growth medium is rapid relative to the oxidation rate ($R_{diff,NH3}$ or $R_{diff,NH4} > R_{AMO}$) and enzymatic ammonia oxidation is the rate-limiting step. In this scenario, the enzyme-level isotope effect ($^{15}\varepsilon_{AMO}$), plus the equilibrium isotope effect between $NH_3$ and $NH_4^+$ ($^{15}\varepsilon_{eq}$ = 19‰; (Hermes *et al.*, 1985), should dominate the observed $^{15}\varepsilon_{NH3}$ early in the experiment. In the later stages of growth, the reaction may become diffusion limited ($R_{diff} < R_{AMO}$) and the isotope effect for diffusion ($^{15}\varepsilon_{diff}$) would dominate. A similar mechanism has been examined for variations in expressed isotopic fractionation during $NH_4^+$ assimilation by bacteria (Hoch *et al.*, 1992) and marine algae (Pennock *et al.*, 1996), as well as $CO_2$

uptake by algae (Laws *et al.*, 1997) and plants (O'Leary, 1981). Diffusion of $NH_3$ in aqueous solution is estimated to have an isotope effect of 20‰ (Hoch *et al.*, 1992), which is similar to the late-stage $^{15}\varepsilon_{NH3}$ values we observed. However, this scenario would predict a direct relationship between [$NH_4^+$] and $^{15}\varepsilon_{NH3}$ in experiments starting at different initial $NH_4^+$ concentrations, which is not observed in our data (Table 2). If anything, we observe larger $^{15}\varepsilon_{NH3}$ values at low initial [$NH_4^+$]. Therefore, we reject the hypothesis of diffusion limitation in controlling $^{15}\varepsilon_{NH3}$ in these experiments.

It has been assumed here that the Amo-catalyzed reaction occurs in the periplasm, as it does in AOB, and that active transport of $NH_3$ or $NH_4^+$ into the periplasm from the medium does not occur. Genes for putative Amt transporters have been identified in the genomes of both AOB (Arp *et al.*, 2007) and AOA (Blainey *et al.*, 2011; Hallam *et al.*, 2006; Walker *et al.*, 2010) and expression of these genes in environmental samples appears proportional to expression of *amo* genes (Stewart *et al.*, 2011). At this time it is uncertain whether Amt supplies N for anabolic metabolism serves a regulatory function (Arp *et al.*, 2007), or supplies substrate to the Amo enzyme. However, if Amt is localized for transport across the cytoplasmic membrane (Andrade *et al.*, 2005), it would be difficult to envision a role for Amt in the $^{15}\varepsilon_{NH3}$ variations observed here.

A second hypothesis to explain the within-experiment variations in $^{15}\varepsilon_{NH3}$ is that during early exponential phase growth, the first step of ammonia oxidation proceeds more quickly than the second step ($R_{AMO} > R_2$) and an as-yet unknown intermediate ($NH_2OH$ or HNO) accumulates. This intermediate pool would be isotopically depleted relative to $NH_4^+$ outside the cell, and a second isotope effect would be expressed ($^{15}\varepsilon_2$; Figure 6) resulting in the production of $NO_2^-$ with a large apparent isotope effect. If the

intermediate pool is eventually used up and ammonia oxidation proceeds as a pseudo one-step reaction, the apparent isotope effect should decrease to $^{15}\varepsilon_{AMO}$ (plus $^{15}\varepsilon_{eq}$) late in the experiment. This hypothesis is consistent with the fact that curvature in the Rayleigh plots was most prominent where long lag phases preceded ammonia oxidation, which may be associated with imbalanced growth early in the experiment. Interestingly, if this hypothesis is correct, the similarity between average $^{15}\varepsilon_{NH3}$ (22‰) and $^{15}\varepsilon_{eq}$ (19‰); (Hermes *et al.*, 1985)) may indicate a small kinetic isotope effect for Amo. Use of the Rayleigh distillation equation with measurements of $\delta^{15}N_{NH4}$ would get around the potential problem from accumulation of intermediates, although it would still be affected by $NH_3/NH_4^+$ equilibration and $NH_4^+$ transport effects discussed above. At this time there are many additional uncertainties in the archaeal ammonia oxidation pathway (Klotz and Stein, 2008; Walker *et al.*, 2010) including the exact chemical intermediates, the localization of the respiratory enzymes within the cell, and the role of active $NH_3/NH_4^+$ transport that must be resolved before the mechanisms causing variable $^{15}\varepsilon_{NH3}$ can be fully explained.

The ultimate goal of determining species-level isotope effects is to better interpret natural abundance stable isotope ratios ($\delta^{15}N_{NO3}$ and $\delta^{18}O_{NO3}$) in the environment. The average $\delta^{15}N$ of marine $NO_3^-$ is set by the balance of $N_2$ fixation and N removal by denitrification and anammox (Brandes and Devol, 2002), although nitrification can affect the partitioning of $^{15}N$ between dissolved and particulate N (Wankel et al., 2007). The potential for variable $^{15}\varepsilon_{NH3}$ adds an extra level of complexity to the interpretations of $\delta^{15}N_{NO3}$ in the environment.

Nitrification is also the main determinant in setting the average $\delta^{18}O$ of marine $NO_3^-$ (Casciotti *et al.*, 2002; Sigman *et al.*, 2009) and nitrous oxide ($N_2O$) (Ostrom *et al.*, 2000; Popp *et al.*, 2002). Determining the oxygen isotope effects for archaeal ammonia oxidation will therefore be an important next step in advancing the use of the dual isotope signatures of $NO_3^-$ and $N_2O$ to understand the marine nitrogen cycle.

**Acknowledgments**

This work was supported by a Woods Hole Oceanographic Institution (WHOI) Postdoctoral Scholar fellowship to AES and the WHOI Ocean Life Institute. We thank Josh Plant and Ken Johnson for the $NH_4^+$ concentration data from cruise CN107, and Christopher Francis for logistical support during that cruise. Matt McIlvin is acknowledged for expert technical assistance with mass spectrometry. Cornelia Wuchter is acknowledged for assistance with the CARD-FISH procedure. Louis Kerr at the Marine Biological Laboratory microscopy facility assisted with the fluorescence micrographs. We thank Stefan Sievert and Matt Johnson for access to equipment in their laboratories. Carolyn Buchwald, Edward Leadbetter, and three anonymous reviewers provided invaluable comments on the manuscript.

**Figure Legends**

Figure 1. Fluorescence microscopy images of enrichment CN25 stained with (a) DAPI and (b) CARD-FISH using the Cren537-554 probe suite. Both images are from the same field of view; the scale bar represents 5 µm.

Figure 2. Phylogenetic placement of the CN enrichments based on (a) 16S rRNA gene sequences (1,268 nucleotide positions) and (b) *amoA* gene sequences (489 nucleic acid positions). The CN enrichment sequences are shown in bold. Trees were constructed using maximum likelihood methods (RAxML) using *Sulfolobus solfataricus* as the outgroup for the 16S rRNA tree and the soil and hot spring sequences as the outgroup for the *amoA* tree. Bootstrap support values (>70%) are shown at nodes; some values have been removed from minor nodes for clarity.

Figure 3. Growth of enrichment CN75 in ONP medium. Error bars denote one standard deviation and in some cases are smaller than the point.

Figure 4. Ammonia oxidation by CN25 in the presence of 10 and 100 µg $mL^{-1}$ allylthiourea (ATU). Each point represents the mean of three replicate bottles; error bars denote one standard deviation from the mean.

Figure 5. $\delta^{15}N_{NO2}$ during ammonia oxidation in batch culture for the archaeal enrichments (a) CN25, (b) CN75, and (c) CN150. Kinetic isotope effects for ammonia oxidation ($^{15}\varepsilon_{NH3}$) were calculated using linear regression of $\delta^{15}N_{NO2}$ vs. $f * \ln(f)/(1-f)$ as described in the text and are reported in Table 2. $f$ is the fraction of the initial [$NH_4^+$] remaining in the culture.

Figure 6. Potential pathways of $NH_3$ acquisition and oxidation by ammonia-oxidizing archaea that could lead to a variable kinetic isotope effect ($^{15}\varepsilon_{NH3}$) (Walker *et al.*, 2010).

$R_{eq}$ and $^{15}\varepsilon_{eq}$ are the rate and equilibrium isotope effect for $NH_3/NH_4^+$ equilibration, $R_{diff,NH4}$ and $^{15}\varepsilon_{diff,NH4}$ are the rate and kinetic isotope effect for $NH_4^+$ diffusion, $R_{diff,NH3}$ and $^{15}\varepsilon_{diff,NH3}$ are the rate and kinetic isotope effect for $NH_3$ diffusion, $R_{AMO}$ and $^{15}\varepsilon_{AMO}$ are the rate and kinetic isotope effect for ammonia oxidation by ammonia monooxygenase (Amo), and $R_2$ and $^{15}\varepsilon_2$ are the rate and kinetic isotope effect for the second step of the ammonia oxidation pathway. Major uncertainties in the archaeal oxidation pathway are shown in red.

Supplemental Figure 1. Phylogenetic tree of 87 archaeal amoA sequences chosen to illustrate the relationship between the CN enrichments (shown in red), cultivated ammonia-oxidizing archaea, and environmental sequences from the enrichment site and other Pacific locations. This Jukes-Cantor distance based tree is based on a 489 base pair alignment of the *amoA* gene.

Table 1. *In situ* conditions for the starting material for North Pacific Ocean seawater enrichments used for archaeal kinetic isotope fractionation ($^{15}\varepsilon_{NH3}$) determination.

| Enrichment | Depth (m) | Temp (ºC) | $[NH_4^+]$ (nmol $L^{-1}$) | $[NO_3^-]$ (µmol $L^{-1}$) |
|---|---|---|---|---|
| CN25 | 25 | 14 | 40 | 0.5 |
| CN75 | 75 | 12 | <15 | 2.2 |
| CN150 | 150 | 10 | <15 | 15.1 |

Table 2. Experimental results for kinetic isotope effect ($^{15}\varepsilon_{NH3}$) determinations during of archaeal ammonia oxidation. CI 95% is the 95% confidence interval. [N+N] is the sum of the measured [$NH_4^+$] and [$NO_2^-$]. SD is standard deviation.

| Enrichment | Experiment # | $^{15}\varepsilon_{NH3}$ (‰) | CI 95% (‰) | Initial [$NH_4^+$] (μmol $L^{-1}$) | $[N+N]_{final}$:$[N+N]_{initial}$ | $NH_4^+$ oxidation rate[a] (μmol $L^{-1}$ $d^{-1}$) |
|---|---|---|---|---|---|---|
| CN25 | 1 | 25 | 1 | 15 | 1.05 | 3.0 |
| | | 28 | 28 | 15 | 1.05 | 2.5 |
| | | 30 | 83 | 15 | 1.05 | 2.1 |
| | 2 | 25 | 52 | 9 | 0.99 | 0.4 |
| | 3 | 26 | 21 | 16 | 0.74 | 0.8 |
| | | 14 | 4 | 16 | 0.98 | 0.9 |
| | | 15 | 3 | 14 | 1.07 | 0.4 |
| | 4 | 20 | 7 | 76 | 1.03 | 4.5 |
| | | 21 | 6 | 77 | 1.02 | 4.5 |
| | | 20 | 4 | 77 | 1.02 | 4.5 |
| | | 20 | 4 | 76 | 0.97 | 4.4 |
| | mean ± SD | 22 ± 5‰ | | | | |
| CN75 | 1 | 37 | 58 | 10 | 0.81 | 0.4 |
| | | 20 | 5 | 10 | 1.05 | 0.4 |
| | | 14 | NaN[b] | 9 | 1.07 | 0.5 |
| | 2 | 23 | 20 | 16 | 0.90 | 0.8 |
| | | 19 | 11 | 17 | 0.90 | 0.9 |
| | | 10 | 8 | 14 | 1.06 | 0.2 |
| | mean ± SD | 21 ± 10‰ | | | | |
| CN150 | 1 | 16 | 3 | 25 | 1.04 | 0.4 |
| | | 20 | 1 | 25 | 1.03 | 0.6 |
| | 2 | 18 | 4 | 46 | 0.94 | 3.4 |
| | | 28 | 17 | 48 | 0.88 | 1.7 |
| | 3 | 23 | 2 | 49 | 0.90 | 4.1 |
| | | 28 | 4 | 50 | 0.88 | 4.5 |
| | | 22 | 4 | 52 | 0.85 | 3.7 |
| | mean ± SD | 22 ± 5‰ | | | | |

[a]Approximate $NH_4^+$ oxidation rates were calculated from the change in [$NO_2^-$] and the time elapsed between the first and final timepoints, and may underestimate the actual rate in experiments where the final time point was after all $NH_4^+$ had been consumed.

[b]Calculating a confidence interval was not possible for this experiment because only two points were

2 available to calculate the slope.

## References


Andrade SLA, Dickmanns A, Ficner R, Einsle O (2005). Crystal structure of the archaeal ammonium transporter Amt-1 from Archaeoglobus fulgidus. *Proc Natl Acad Sci U S A* **102:** 14994.

Arp DJ, Chain PSG, Klotz MG (2007). The Impact of Genome Analyses on Our Understanding of Ammonia-Oxidizing Bacteria*. *Microbiology* **61:** 503.

Balch WE, Fox GE, Magrum LJ, Woese CR, Wolfe RS (1979). Methanogens - Re-evaluation of a unique biological group. *Microbiol Rev* **43:** 260-296.

Bedard C, Knowles R (1989). Physiology, biochemistry, and specific inhibitors of CH4, NH4+, and CO oxidation by methanotrophs and nitrifiers. *Microbiol Mol Biol Rev* **53:** 68.

Beman JM, Popp BN, Francis CA (2008). Molecular and biogeochemical evidence for ammonia oxidation by marine Crenarchaeota in the Gulf of California. *ISME Journal* **2:** 429-441.

Beman JM, Sachdeva R, Fuhrman JA (2010). Population ecology of nitrifying Archaea and Bacteria in the Southern California Bight. *Environ Microbiol* **12:** 1282-1292.

Bernhard AE, Landry ZC, Blevins A, de la Torre JR, Giblin AE, Stahl DA (2010). Abundance of ammonia-oxidizing archaea and bacteria along an estuarine salinity gradient in relationship to potential nitrification rates. *Appl Environ Microbiol* **76:** 1285-1289.

Blainey PC, Mosier AC, Potanina A, Francis CA, Quake SR, Gilbert J (2011). Genome of a Low-Salinity Ammonia-Oxidizing Archaeon Determined by Single-Cell and Metagenomic Analysis. *PLoS One* **6:** 148-149.

Brandes JA, Devol AH (2002). A global marine-fixed nitrogen isotopic budget: Implications for Holocene nitrogen cycling. *Global Biogeochemical Cycles* **16:** 1120.

Brochier-Armanet C, Boussau B, Gribaldo S, Forterre P (2008). Mesophilic crenarchaeota: proposal for a third archaeal phylum, the Thaumarchaeota. *Nature Reviews Microbiology* **6:** 245-252.

Buchwald C, Casciotti KL (2010). Oxygen isotopic fractionation and exchange during bacterial nitrite oxidation. *Limnol Oceanogr* **55:** 1064-1074.

Casciotti KL (2009). Inverse kinetic isotope fractionation during bacterial nitrite oxidation. *Geochimica Et Cosmochimica Acta* **73:** 2061-2076.

Casciotti KL, Bohlke JK, McIlvin MR, Mroczkowski SJ, Hannon JE (2007). Oxygen isotopes in nitrite: Analysis, calibration, and equilibration. *Anal Chem* **79:** 2427-2436.

Casciotti KL, Buchwald C, Santoro AE, Frame C (2011). Assessment of nitrogen and oxygen isotope fraction during nitrification and its expression in the marine environment. *Methods Enzymol* **483**.

Casciotti KL, McIlvin MR, Buchwald C (2010). Oxygen isotopic exchange and fractionation during bacterial ammonia oxidation. *Limnol Oceanogr* **55:** 753-762.

Casciotti KL, Sigman DM, Hastings MG, Bohlke JK, Hilkert A (2002). Measurement of the oxygen isotopic composition of nitrate in seawater and freshwater using the denitrifier method. *Anal Chem* **74:** 4905-4912.

Casciotti KL, Sigman DM, Ward BB (2003). Linking diversity and stable isotope fractionation in ammonia-oxidizing bacteria. *Geomicrobiology Journal* **20:** 335-353.

Casciotti KL, Trull TW, Glover DM, Davies D (2008). Constraints on nitrogen cycling at the subtropical North Pacific Station ALOHA from isotopic measurements of nitrate and particulate nitrogen. *Deep Sea Res* **55:** 1661-1672.

Church MJ, Karl DM, DeLong EF (2010). Abundances of crenarchaeal amoA genes and transcripts in the Pacific Ocean. *Environ Microbiol* **12:** 679-688.

Clark DR, Rees AP, Joint I (2008). Ammonium regeneration and nitrification rates in the oligotrophic Atlantic Ocean: Implications for new production estimates. *Limnol Oceanogr* **53:** 52-62.

Coolen MJL, Abbas B, van Bleijswijk J, Hopmans EC, Kuypers MMM, Wakeham SG *et al* (2007). Putative ammonia-oxidizing Crenarchaeota in suboxic waters of the Black Sea: a basin-wide ecological study using 16S ribosomal and functional genes and membrane lipids. *Environ Microbiol* **9:** 1001-1016.

de la Torre JR, Walker CB, Ingalls AE, Koenneke M, Stahl DA (2008). Cultivation of a thermophilic ammonia oxidizing archaeon synthesizing crenarchaeol. *Environ Microbiol* **10:** 810-818.

Delong EF (1992). Archaea in coastal marine environments. *Proc Natl Acad Sci U S A* **89:** 5685-5689.

DiFiore PJ, Sigman DM, Dunbar RB (2009). Upper ocean nitrogen fluxes in the Polar Antarctic Zone: Constraints from the nitrogen and oxygen isotopes of nitrate. *Geochemistry Geophysics Geosystems* **10:** Q11016.

Eppley RW, Peterson BJ (1979). Particulate organic matter flux and planktonic new production in the deep ocean. *Nature* **282:** 677.

Francis CA, Roberts KJ, Beman JM, Santoro AE, Oakley BB (2005). Ubiquity and diversity of ammonia-oxidizing archaea in water columns and sediments of the ocean. *Proc Natl Acad Sci U S A* **102:** 14683-14688.

Ginestet P, Audic JM, Urbain V, Block JC (1998). Estimation of nitrifying bacterial activities by measuring oxygen uptake in the presence of the metabolic inhibitors allylthiourea and azide. *Appl Environ Microbiol* **64:** 2266-2268.

Granger J, Sigman DM, Lehmann MF, Tortell PD (2008). Nitrogen and oxygen isotope fractionation during dissimilatory nitrate reduction by denitrifying bacteria. *Limnol Oceanogr* **53:** 2533-2545.

Granger J, Sigman DM, Needoba JA, Harrison PJ (2004). Coupled nitrogen and oxygen isotope fractionation of nitrate during assimilation by cultures of marine phytoplankton. *Limnol Oceanogr* **49:** 1763-1773.

Habicht K, Salling L, Thamdrup B, Canfield D (2005). Effect of low sulfate concentrations on lactate oxidation and isotope fractionation during sulfate reduction by Archaeoglobus fulgidus strain Z. *Appl Environ Microbiol* **71:** 3770.

Hallam SJ, Mincer TJ, Schleper C, Preston CM, Roberts K, Richardson PM *et al* (2006). Pathways of carbon assimilation and ammonia oxidation suggested by environmental genomic analyses of marine Crenarchaeota. *PLoS Biology* **4:** 520-536.

Hatzenpichler R, Lebecleva EV, Spieck E, Stoecker K, Richter A, Daims H *et al* (2008). A moderately thermophilic ammonia-oxidizing crenarchaeote from a hot spring. *Proc Natl Acad Sci U S A* **105**.

Hermes JD, Weiss PM, Cleland W (1985). Use of nitrogen-15 and deuterium isotope effects to determine the chemical mechanism of phenylalanine ammonia-lyase. *Biochemistry* **24:** 2959-2967.

Hoch MP, Fogel ML, Kirchman DL (1992). Isotope fractionation associated with ammonium uptake by a marine bacterium. *Limnol Oceanogr* **37:** 1447-1459.

Holmes RM, Aminot A, Kèrouel R, Hooker BA, Peterson BJ (1999). A simple and precise method for measuring ammonium in marine and freshwater ecosystems. *Canadian Journal of Fisheries and Aquatic Sciences* **56:** 1801-1808.

Hooper AB, Terry KR (1973). Specific inhibitors of ammonia oxidation in Nitrosomonas. *J Bacteriol* **115:** 480.

Hyman MR, Wood P (1985). Suicidal inactivation and labelling of ammonia mono-oxygenase by acetylene. *Biochem J* **227:** 719.

Johnson KS, Boyle E, Bruland K, Coale K, Measures C, Moffett J *et al* (2007). The SAFe iron intercomparison cruise: An international collaboration to develop dissolved iron in seawater standards *EOS Transactions of the American Geophysical Union* **88:** 131-132.

Klotz MG, Stein LY (2008). Nitrifier genomics and evolution of the nitrogen cycle. *FEMS Microbiology Letters* **278:** 146-156.

Konneke M, Bernhard AE, de la Torre JR, Walker CB, Waterbury JB, Stahl DA (2005). Isolation of an autotrophic ammonia-oxidizing marine archaeon. *Nature* **437:** 543-546.

Lam P, Jensen MM, Lavik G, McGinnis DF, Muller B, Schubert CJ *et al* (2007). Linking crenarchaeal and bacterial nitrification to anammox in the Black Sea. *Proc Natl Acad Sci U S A* **104:** 7104-7109.

Lam P, Lavik G, Jensen MM, van de Vossenberg J, Schmid M, Woebken D *et al* (2009). Revising the nitrogen cycle in the Peruvian oxygen minimum zone. *Proceedings of the National Academy of Sciences* **106:** 4752.

Laws EA, Bidigare RR, Popp BN (1997). Effect of growth rate and CO 2 concentration on carbon isotopic fractionation by the marine diatom Phaeodactylum tricornutum. *Limnol Oceanogr* **42:** 1552-1560.

Ludwig W, Strunk O, Westram R, Richter L, Meier H, Yadhukumar *et al* (2004). ARB: a software environment for sequence data. *Nucleic Acids Res* **32:** 1363-1371.

Mariotti A, Germon JC, Hubert P, Kaiser P, Letolle R, Tardieux A *et al* (1981). Experimental determination of nitrogen kinetic isotope fractionation: some principles; illustration for the denitrification and nitrification processes. *Plant and Soil* **62:** 413-430.

Martens-Habbena W, Berube PM, Urakawa H, de la Torre JR, Stahl DA (2009). Ammonia oxidation kinetics determine niche separation of nitrifying Archaea and Bacteria. *Nature* **461:** 976-981.

McIlvin MR, Altabet MA (2005). Chemical conversion of nitrate and nitrite to nitrous oxide for nitrogen and oxygen isotopic analysis in freshwater and seawater. *Anal Chem* **77:** 5589-5595.

McIlvin MR, Casciotti KL (2010). Fully automated system for stable isotopic analysis of dissolved nitrous oxide at natural abundance levels. *Limnology and Oceanography Methods* **8:** 54-66.

McIlvin MR, Casciotti KL (2011). Technical updates to the bacterial method for nitrate isotopic analyses. *Anal Chem***:** doi: 10.1021/ac1028984.

Mincer TJ, Church MJ, Taylor LT, Preston C, Karl DM, DeLong EF (2007). Quantitative distribution of presumptive archaeal and bacterial nitrifiers in Monterey Bay and the North Pacific Subtropical Gyre. *Environ Microbiol* **9:** 1162-1175.

Morris JJ, Kirkegaard R, Szul MJ, Johnson ZI, Zinser ER (2008). Facilitation of robust growth of Prochlorococcus colonies and dilute liquid cultures by" helper" heterotrophic bacteria. *Appl Environ Microbiol* **74:** 4530.

Mosier AC, Francis CA (2008). Relative abundance and diversity of ammonia-oxidizing archaea and bacteria in the San Francisco Bay estuary. *Environ Microbiol* **10:** 3002-3016.

Needoba JA, Waser NA, Harrison PJ, Calvert SE (2003). Nitrogen isotope fractionation in 12 species of marine phytoplankton during growth on nitrate. *Marine Ecology Progress Series* **255:** 81-91.

O'Leary MH (1981). Carbon isotope fractionation in plants. *Phytochemistry* **20:** 553-567.

Olson RJ (1981). 15 N tracer studies of the primary nitrite maximum. *J Mar Res* **39:** 203-226.

Ostrom NE, Russ ME, Popp BN, Rust TM, Karl DM (2000). Mechanisms of nitrous oxide production in the subtropical North Pacific based on determinations of the isotopic abundances of nitrous oxide and di-oxygen. *Chemosphere-Global Change Science* **2:** 281-290.

Pennock JR, Velinsky DJ, Ludlam JM, Sharp JH, Fogel ML (1996). Isotopic fractionation of ammonium and nitrate during uptake by Skeletonema costatum: Implications for 15N dynamics under bloom conditions. *Limnol Oceanogr* **41:** 451-459.

Popp BN, Westley MB, Toyoda S, Miwa T, Dore JE, Yoshida N *et al* (2002). Nitrogen and oxygen isotopomeric constraints on the origins and sea-to-air flux of N2O in the oligotrophic subtropical North Pacific gyre. *Global Biogeochemical Cycles* **16:** 1064, doi: 10.1029/2001GB001806.

Prosser JI (1990). Autotrophic nitrification in bacteria. *Adv Microb Physiol* **30:** 125-181.

Pruesse E, Quast C, Knittel K, Fuchs B, Ludwig W, Peplies J *et al* (2007). SILVA: a comprehensive online resource for quality checked and aligned ribosomal RNA sequence data compatible with ARB. *Nucleic Acids Res* **35:** 7188.

Purkhold U, Pommerening-Roser A, Juretschko S, Schmid MC, Koops HP, Wagner M (2000). Phylogeny of all recognized species of ammonia oxidizers based on comparative 16S rRNA and amoA sequence analysis: Implications for molecular diversity surveys. *Appl Environ Microbiol* **66:** 5368-5382.

Rusch DB, Halpern AL, Sutton G, Heidelberg KB, Williamson S, Yooseph S *et al* (2007). The Sorcerer II Global Ocean Sampling expedition: Northwest Atlantic through Eastern Tropical Pacific. *Plos Biology* **5:** 398-431.

Santoro AE, Casciotti KL, Francis CA (2010). Activity, abundance and diversity of nitrifying archaea and bacteria in the central California Current. *Environ Microbiol* **12:** 1989-2006.

Santoro AE, Francis CA, de Sieyes NR, Boehm AB (2008). Shifts in the relative abundance of ammonia-oxidizing bacteria and archaea across physicochemical gradients in a subterranean estuary. *Environ Microbiol* **10:** 1068-1079.

Sigman DM, DiFiore PJ, Hain MP, Deutsch C, Wang Y, Karl DM *et al* (2009). The dual isotopes of deep nitrate as a constraint on the cycle and budget of oceanic fixed nitrogen. *Deep Sea Research Part I: Oceanographic Research Papers* **56:** 1419-1439.

Sigman DM, Granger J, DiFiore PJ, Lehmann MF, Ho R, Cane G *et al* (2005). Coupled nitrogen and oxygen isotope measurements of nitrate along the eastern North Pacific margin. *Global Biogeochem Cycles* **19:** GB4022.

Spang A, Hatzenpichler R, Brochier-Armanet C, Rattei T, Tischler P, Spieck E *et al* (2010). Distinct gene set in two different lineages of ammonia-oxidizing archaea supports the phylum Thaumarchaeota. *Trends in Microbiology* **18:** 331-340.

Stein JL, Marsh TL, Wu KY, Shizuya H, DeLong EF (1996). Characterization of uncultivated prokaryotes: isolation and analysis of a 40-kilobase-pair genome fragment from a planktonic marine archaeon. *J Bacteriol* **178:** 591.

Stephen JR, Chang YJ, Macnaughton SJ, Kowalchuk GA, Leung KT, Flemming CA *et al* (1999). Effect of toxic metals on indigenous soil beta-subgroup proteobacterium ammonia oxidizer community structure and protection against toxicity by inoculated metal-resistant bacteria. *Appl Environ Microbiol* **65:** 95-101.

Stewart FJ, Ulloa O, DeLong EF (2011). Microbial metatranscriptomics in a permanent marine oxygen minimum zone. *Environ Microbiol***:** doi:10.1111/j.1462-2920.2010.02400.x.

Strickland J, Parsons T (1968). A practical handbook of seawater analysis. *Fisheries Research Board of Canada Bulletin* **167:** 71-75.

Teira E, Reinthaler T, Pernthaler A, Pernthaler J, Herndl GJ (2004). Combining catalyzed reporter deposition-fluorescence in situ hybridization and microautoradiography to detect substrate utilization by bacteria and archaea in the deep ocean. *Appl Environ Microbiol* **70:** 4411.

Templeton AS, Chu KH, Alvarez-Cohen L, Conrad ME (2006). Variable carbon isotope fractionation expressed by aerobic CH4-oxidizing bacteria. *Geochimica Et Cosmochimica Acta* **70:** 1739-1752.

Urakawa H, Martens-Habbena W, Stahl DA (2010). High abundance of ammonia-oxidizing archaea in coastal waters, determined using a modified DNA extraction method. *Appl Environ Microbiol* **76:** 2129.

Venter JC, Remington K, Heidelberg JF, Halpern AL, Rusch D, Eisen JA *et al* (2004). Environmental genome shotgun sequencing of the Sargasso Sea. *Science* **304:** 66-74.

Walker CB, de la Torre JR, Klotz MG, Urakawa H, Pinel N, Arp DJ *et al* (2010). Nitrosopumilus maritimus genome reveals unique mechanisms for nitrification and autotrophy in globally distributed marine crenarchaea. *Proceedings of the National Academy of Sciences* **107:** 8818-8823.

Wankel SD, Kendall C, Pennington JT, Chavez FP, Paytan A (2007). Nitrification in the euphotic zone as evidenced by nitrate dual isotopic composition: Observations from Monterey Bay, California. *Global Biogeochemical Cycles* **21:** GB2009.

Ward BB (2002). Nitrification in aquatic environments. In: Capone DG (ed). *Encyclopedia of Environmental Microbiology*. John Wiley & Sons: New York. pp 2144-2167.

Ward BB, Olson RJ, Perry MJ (1982). Microbial nitrification rates in the primary nitrite maximum off Southern-California. *Deep-Sea Research Part A-Oceanographic Research Papers* **29:** 247-255.

Wuchter C, Abbas B, Coolen MJL, Herfort L, van Bleijswijk J, Timmers P *et al* (2006). Archaeal nitrification in the ocean. *Proc Natl Acad Sci U S A* **103:** 12317-12322.

Yool A, Martin AP, Fernandez C, Clark DR (2007). The significance of nitrification for oceanic new production. *Nature* **447:** 999-1002.

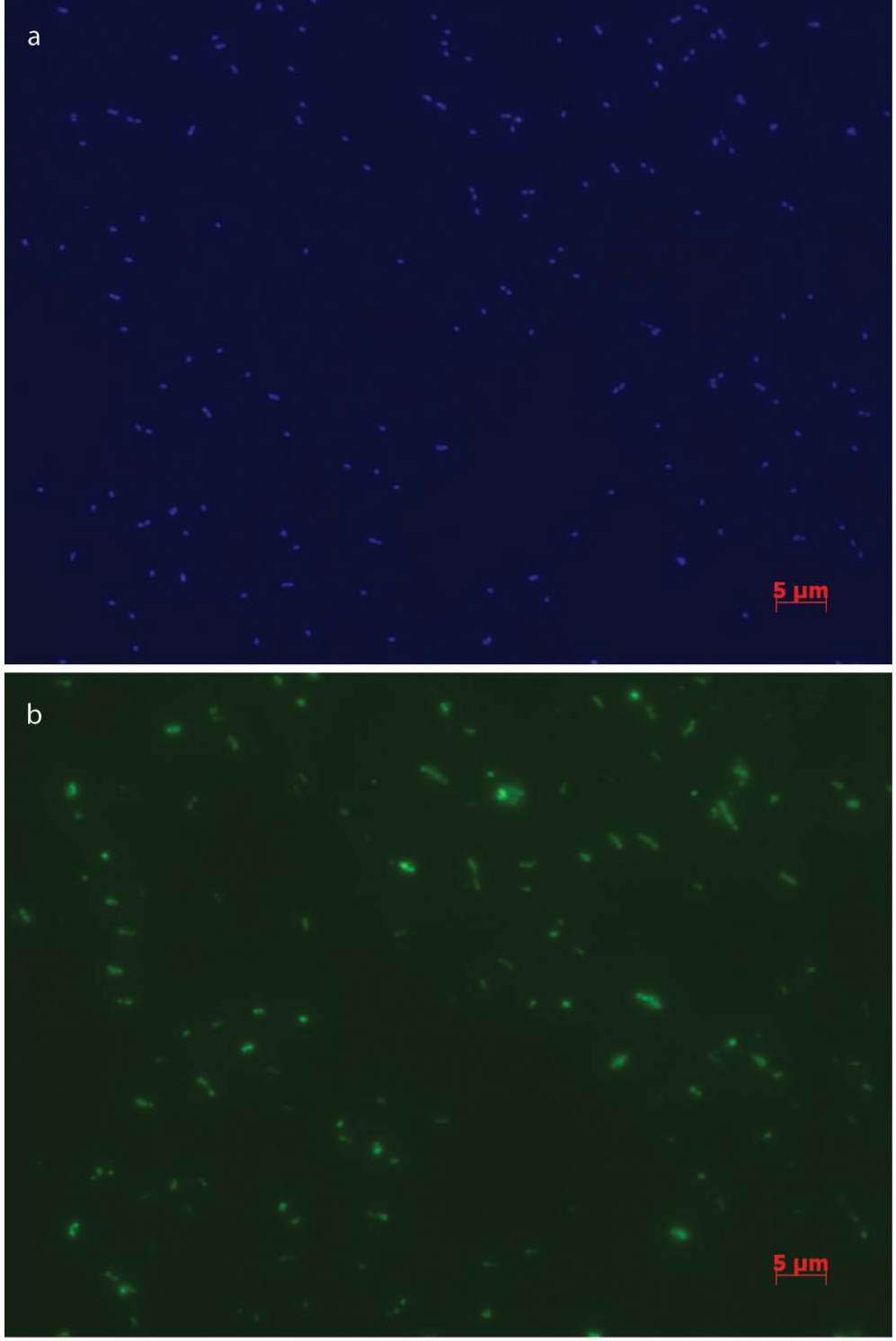


Fig. 1

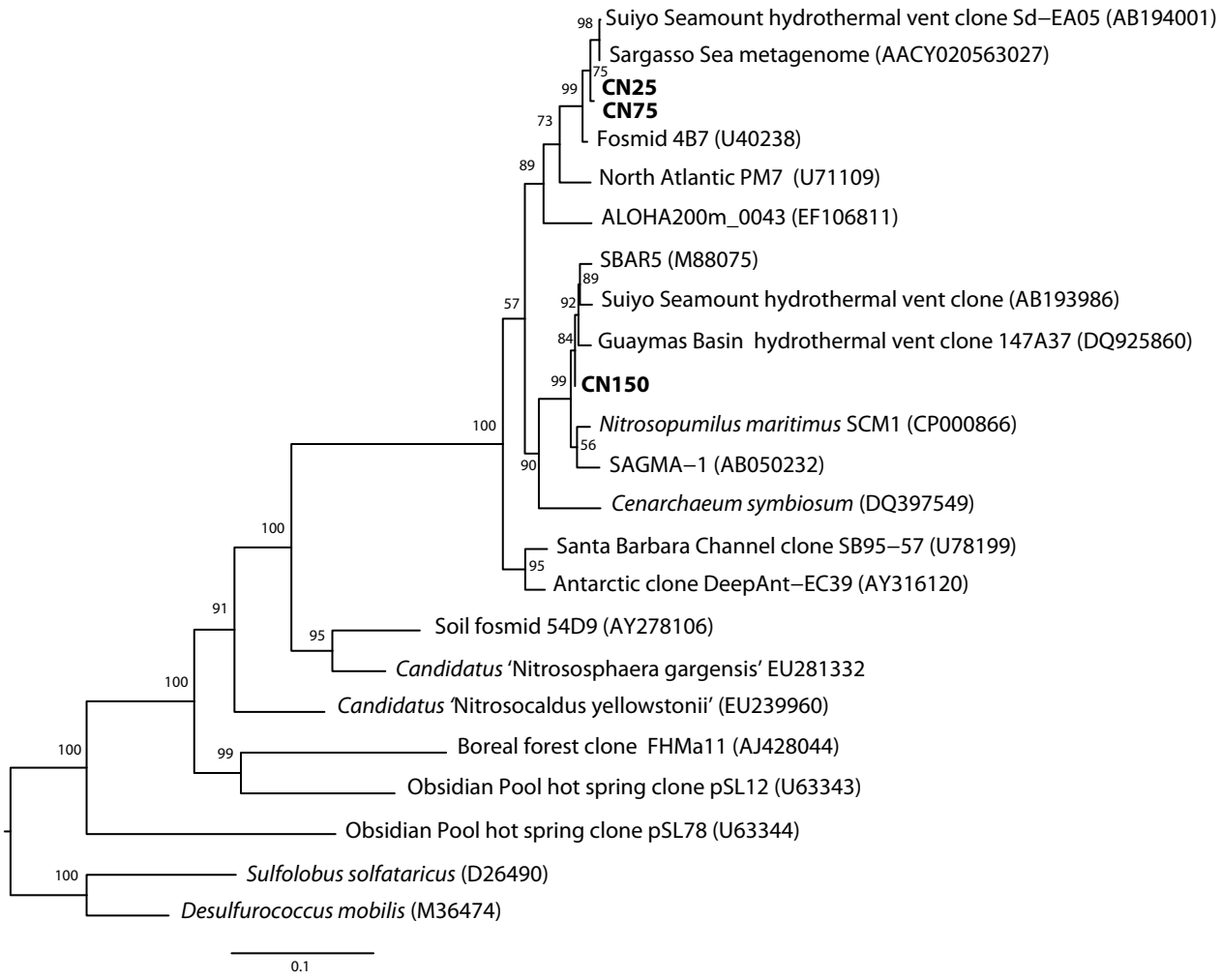
Suiyo Seamount hydrothermal vent clone Sd−EA05 (AB194001)
Sargasso Sea metagenome (AACY020563027)
CN25
CN75
Fosmid 4B7 (U40238)
North Atlantic PM7 (U71109)
ALOHA200m_0043 (EF106811)
SBAR5 (M88075)
Suiyo Seamount hydrothermal vent clone (AB193986)
Guaymas Basin hydrothermal vent clone 147A37 (DQ925860)
CN150
Nitrosopumilus maritimus SCM1 (CP000866)
SAGMA−1 (AB050232)
Cenarchaeum symbiosum (DQ397549)
Santa Barbara Channel clone SB95−57 (U78199)
Antarctic clone DeepAnt−EC39 (AY316120)
Soil fosmid 54D9 (AY278106)
Candidatus 'Nitrososphaera gargensis' EU281332
Candidatus 'Nitrosocaldus yellowstonii' (EU239960)
Boreal forest clone FHMa11 (AJ428044)
Obsidian Pool hot spring clone pSL12 (U63343)
Obsidian Pool hot spring clone pSL78 (U63344)
Sulfolobus solfataricus (D26490)
Desulfurococcus mobilis (M36474)
0.1

Fig. 2a

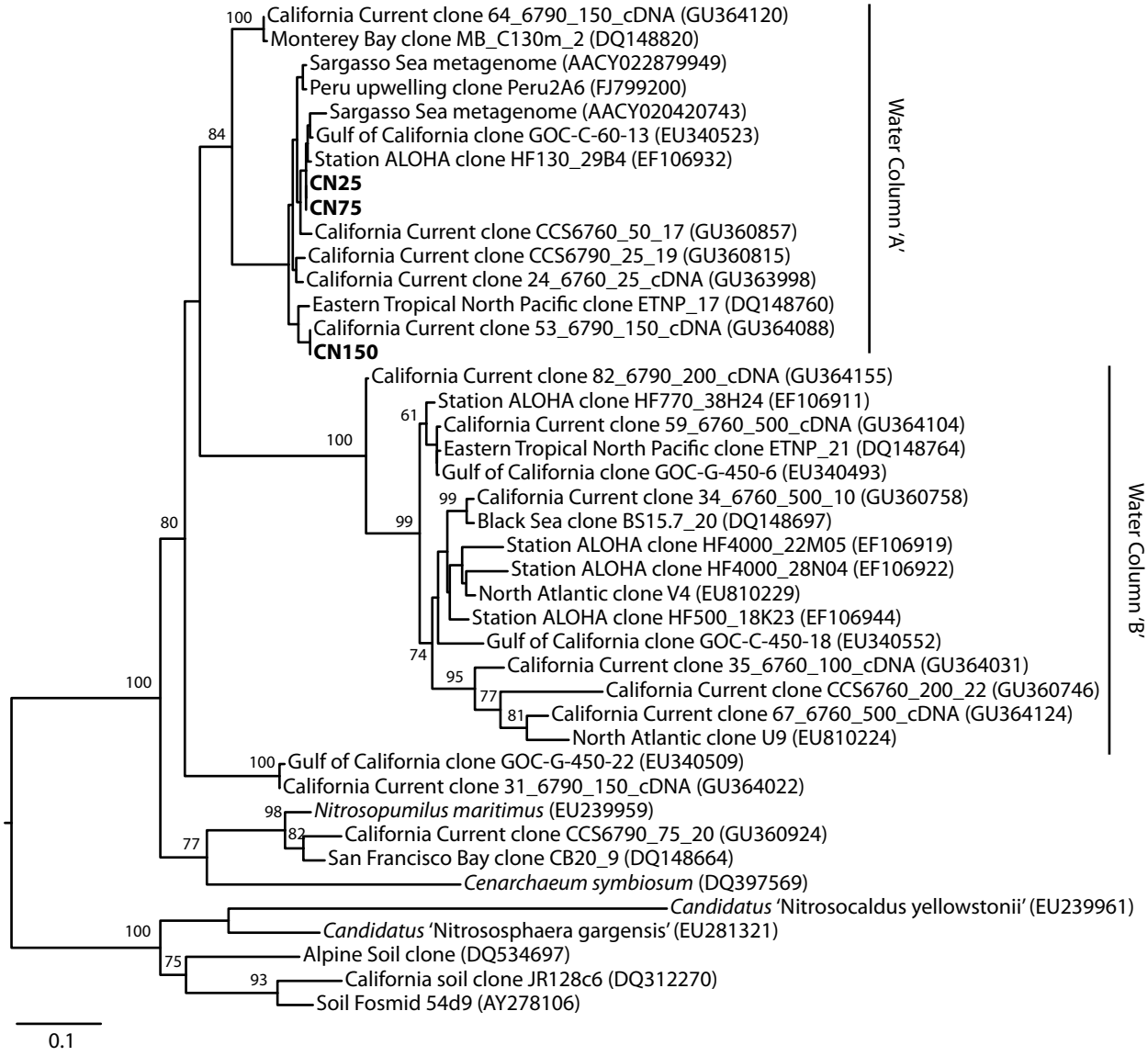
California Current clone 64_6790_150_cDNA (GU364120)
Monterey Bay clone MB_C130m_2 (DQ148820)
Sargasso Sea metagenome (AACY022879949)
Peru upwelling clone Peru2A6 (FJ799200)
Sargasso Sea metagenome (AACY020420743)
Gulf of California clone GOC-C-60-13 (EU340523)
Station ALOHA clone HF130_29B4 (EF106932)
CN25
CN75
California Current clone CCS6760_50_17 (GU360857)
California Current clone CCS6790_25_19 (GU360815)
California Current clone 24_6760_25_cDNA (GU363998)
Eastern Tropical North Pacific clone ETNP_17 (DQ148760)
California Current clone 53_6790_150_cDNA (GU364088)
CN150
Water Column 'A'
California Current clone 82_6790_200_cDNA (GU364155)
Station ALOHA clone HF770_38H24 (EF106911)
California Current clone 59_6760_500_cDNA (GU364104)
Eastern Tropical North Pacific clone ETNP_21 (DQ148764)
Gulf of California clone GOC-G-450-6 (EU340493)
California Current clone 34_6760_500_10 (GU360758)
Black Sea clone BS15.7_20 (DQ148697)
Station ALOHA clone HF4000_22M05 (EF106919)
Station ALOHA clone HF4000_28N04 (EF106922)
North Atlantic clone V4 (EU810229)
Station ALOHA clone HF500_18K23 (EF106944)
Gulf of California clone GOC-C-450-18 (EU340552)
California Current clone 35_6760_100_cDNA (GU364031)
California Current clone CCS6760_200_22 (GU360746)
California Current clone 67_6760_500_cDNA (GU364124)
North Atlantic clone U9 (EU810224)
Water Column 'B'
Gulf of California clone GOC-G-450-22 (EU340509)
California Current clone 31_6790_150_cDNA (GU364022)
Nitrosopumilus maritimus (EU239959)
California Current clone CCS6790_75_20 (GU360924)
San Francisco Bay clone CB20_9 (DQ148664)
Cenarchaeum symbiosum (DQ397569)
Candidatus 'Nitrosocaldus yellowstonii' (EU239961)
Candidatus 'Nitrososphaera gargensis' (EU281321)
Alpine Soil clone (DQ534697)
California soil clone JR128c6 (DQ312270)
Soil Fosmid 54d9 (AY278106)
0.1

Fig. 2b

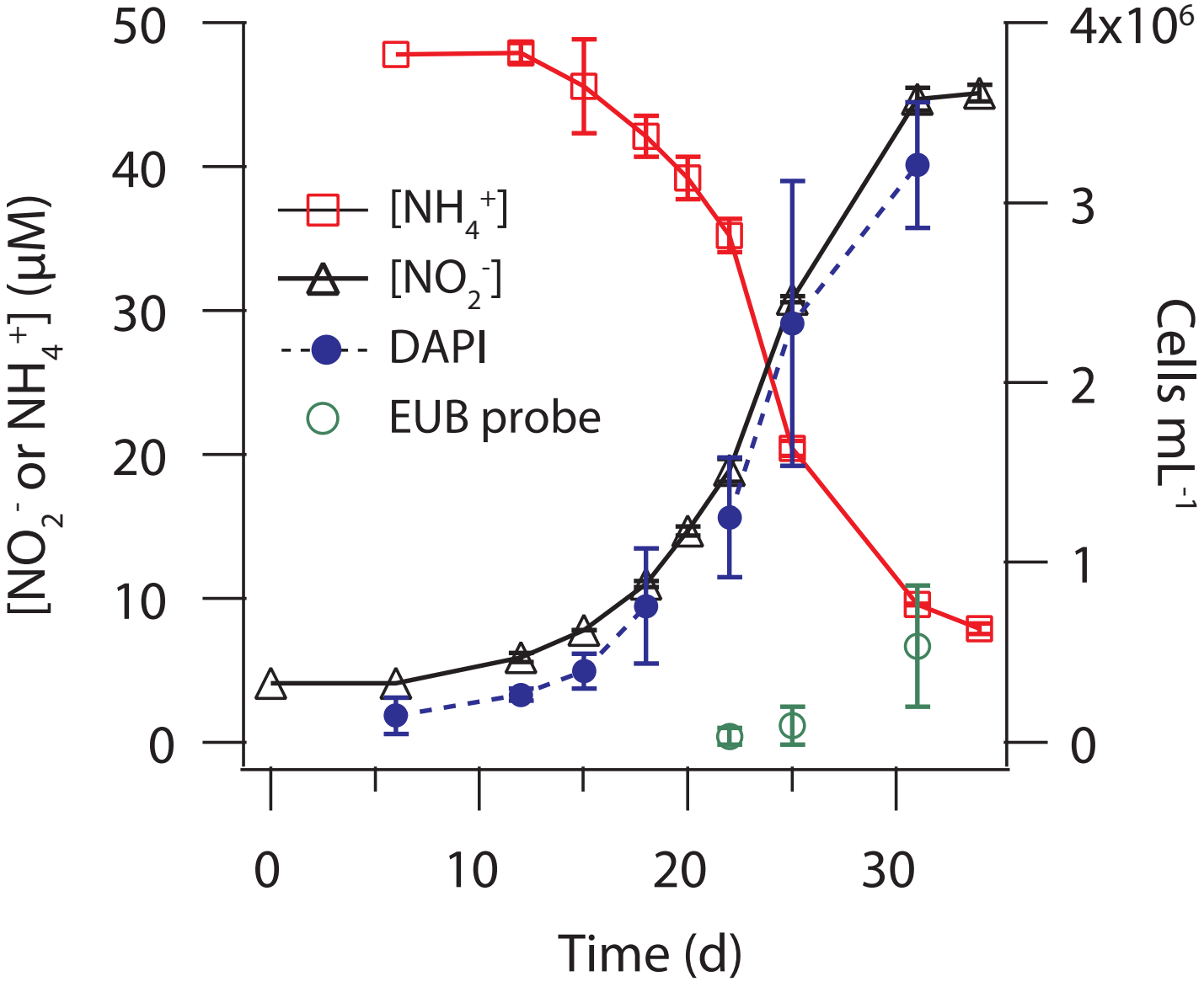
50
40
30
20
10
0
[NO2- or NH4+] (µM)
4x10⁶
3
2
1
0
Cells mL-1
[NH4+]
[NO2-]
DAPI
EUB probe
0
10
20
30
Time (d)

Fig. 3

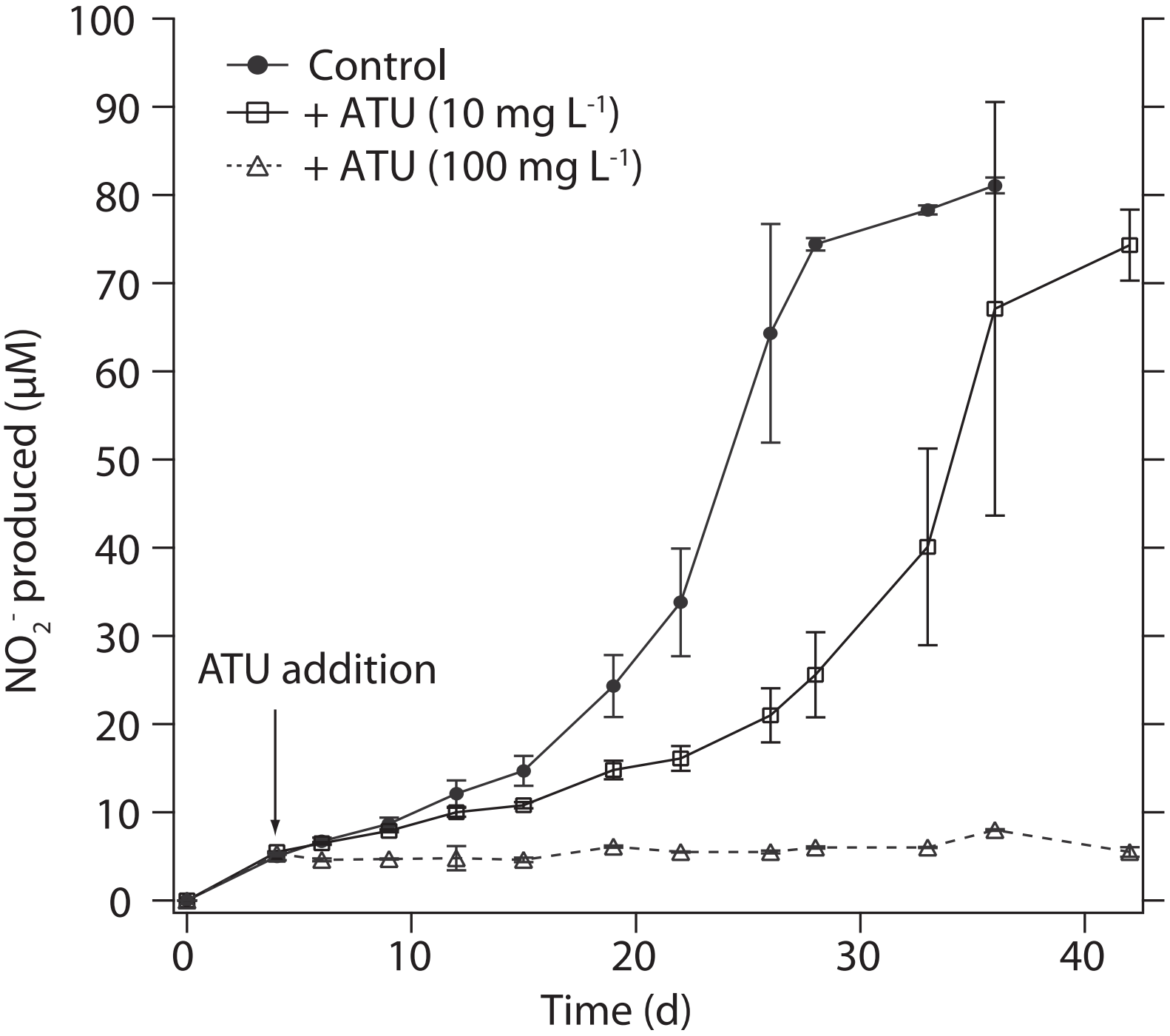
Control
+ ATU (10 mg L-1)
+ ATU (100 mg L-1)
ATU addition
NO2- produced (µM)
Time (d)
0
10
20
30
40
50
60
70
80
90
100

Fig. 4

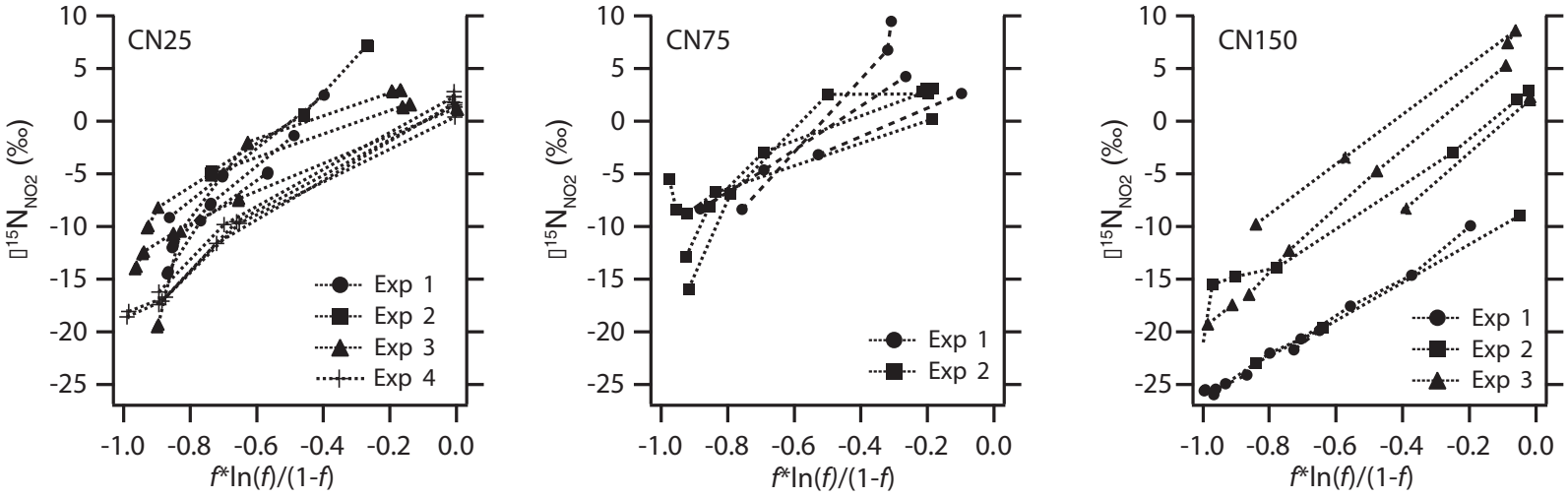
CN25
CN75
CN150
Exp 1
Exp 2
Exp 3
Exp 4
10
5
0
-5
-10
-15
-20
-25
-1.0
-0.8
-0.6
-0.4
-0.2
0.0
f*ln(f)/(1-f)
δ15NNO2 (‰)

Fig. 5

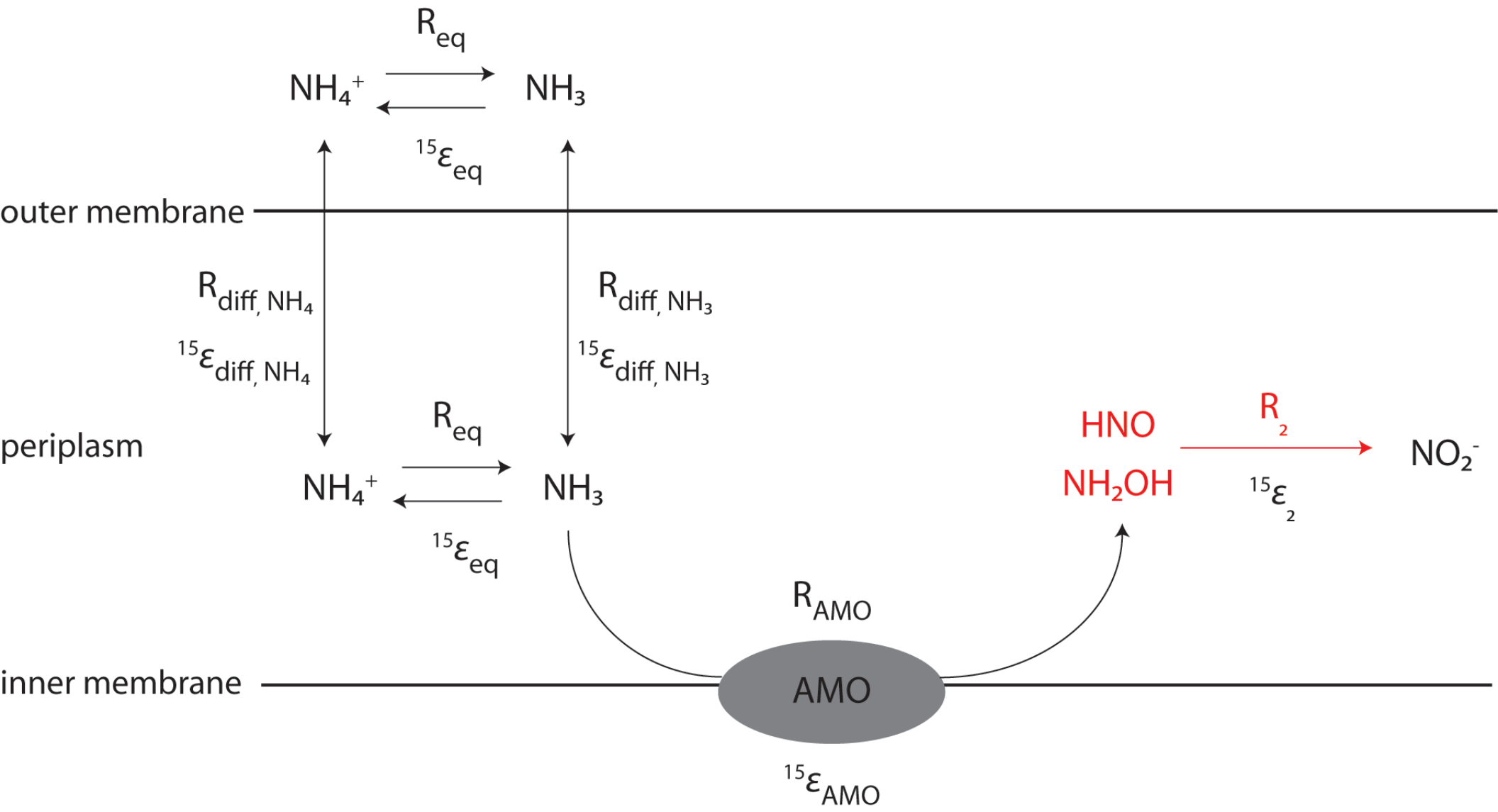
$R_{eq}$
$NH_4^+$
$NH_3$
$^{15}\varepsilon_{eq}$
outer membrane
$R_{diff, NH_4}$
$^{15}\varepsilon_{diff, NH_4}$
$R_{diff, NH_3}$
$^{15}\varepsilon_{diff, NH_3}$
periplasm
$R_{eq}$
$NH_4^+$
$NH_3$
$^{15}\varepsilon_{eq}$
HNO
$NH_2OH$
$R_2$
$^{15}\varepsilon_2$
$NO_2^-$
$R_{AMO}$
AMO
inner membrane
$^{15}\varepsilon_{AMO}$

Fig. 6

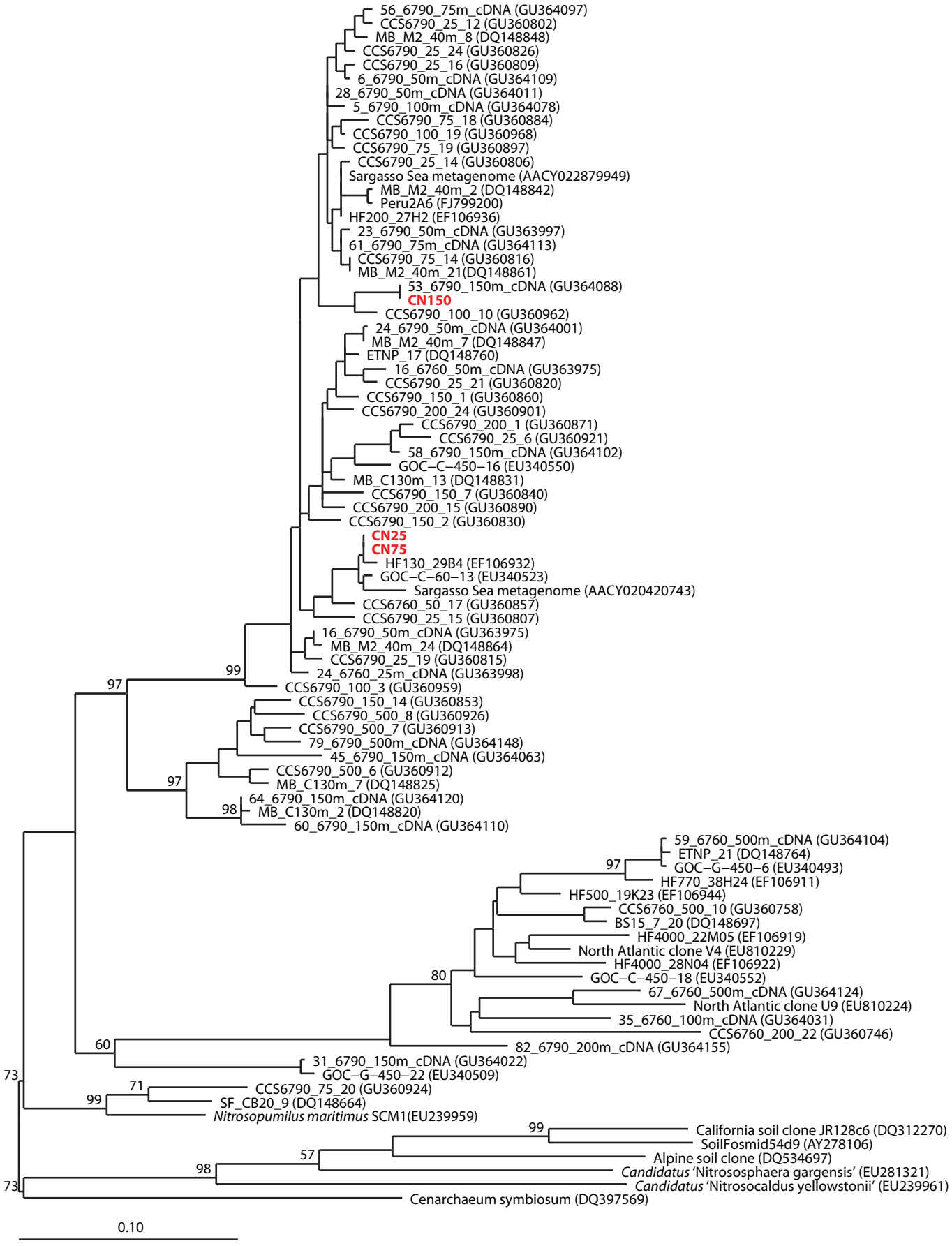
56_6790_75m_cDNA (GU364097)
CCS6790_25_12 (GU360802)
MB_M2_40m_8 (DQ148848)
CCS6790_25_24 (GU360826)
CCS6790_25_16 (GU360809)
6_6790_50m_cDNA (GU364109)
28_6790_50m_cDNA (GU364011)
5_6790_100m_cDNA (GU364078)
CCS6790_75_18 (GU360884)
CCS6790_100_19 (GU360968)
CCS6790_75_19 (GU360897)
CCS6790_25_14 (GU360806)
Sargasso Sea metagenome (AACY022879949)
MB_M2_40m_2 (DQ148842)
Peru2A6 (FJ799200)
HF200_27H2 (EF106936)
23_6790_50m_cDNA (GU363997)
61_6790_75m_cDNA (GU364113)
CCS6790_75_14 (GU360816)
MB_M2_40m_21(DQ148861)
53_6790_150m_cDNA (GU364088)
CN150
CCS6790_100_10 (GU360962)
24_6790_50m_cDNA (GU364001)
MB_M2_40m_7 (DQ148847)
ETNP_17 (DQ148760)
16_6760_50m_cDNA (GU363975)
CCS6790_25_21 (GU360820)
CCS6790_150_1 (GU360860)
CCS6790_200_24 (GU360901)
CCS6790_200_1 (GU360871)
CCS6790_25_6 (GU360921)
58_6790_150m_cDNA (GU364102)
GOC–C–450–16 (EU340550)
MB_C130m_13 (DQ148831)
CCS6790_150_7 (GU360840)
CCS6790_200_15 (GU360890)
CCS6790_150_2 (GU360830)
CN25
CN75
HF130_29B4 (EF106932)
GOC–C–60–13 (EU340523)
Sargasso Sea metagenome (AACY020420743)
CCS6760_50_17 (GU360857)
CCS6790_25_15 (GU360807)
16_6790_50m_cDNA (GU363975)
MB_M2_40m_24 (DQ148864)
CCS6790_25_19 (GU360815)
24_6760_25m_cDNA (GU363998)
CCS6790_100_3 (GU360959)
CCS6790_150_14 (GU360853)
CCS6790_500_8 (GU360926)
CCS6790_500_7 (GU360913)
79_6790_500m_cDNA (GU364148)
45_6790_150m_cDNA (GU364063)
CCS6790_500_6 (GU360912)
MB_C130m_7 (DQ148825)
64_6790_150m_cDNA (GU364120)
MB_C130m_2 (DQ148820)
60_6790_150m_cDNA (GU364110)
59_6760_500m_cDNA (GU364104)
ETNP_21 (DQ148764)
GOC–G–450–6 (EU340493)
HF770_38H24 (EF106911)
HF500_19K23 (EF106944)
CCS6760_500_10 (GU360758)
BS15_7_20 (DQ148697)
HF4000_22M05 (EF106919)
North Atlantic clone V4 (EU810229)
HF4000_28N04 (EF106922)
GOC–C–450–18 (EU340552)
67_6760_500m_cDNA (GU364124)
North Atlantic clone U9 (EU810224)
35_6760_100m_cDNA (GU364031)
CCS6760_200_22 (GU360746)
82_6790_200m_cDNA (GU364155)
31_6790_150m_cDNA (GU364022)
GOC–G–450–22 (EU340509)
CCS6790_75_20 (GU360924)
SF_CB20_9 (DQ148664)
*Nitrosopumilus maritimus* SCM1(EU239959)
California soil clone JR128c6 (DQ312270)
SoilFosmid54d9 (AY278106)
Alpine soil clone (DQ534697)
*Candidatus* 'Nitrososphaera gargensis' (EU281321)
*Candidatus* 'Nitrosocaldus yellowstonii' (EU239961)
Cenarchaeum symbiosum (DQ397569)
99
97
97
98
80
60
73
71
99
99
57
98
73
0.10